Biolability of Fresh and Photodegraded Pyrogenic Dissolved Organic Matter from Laboratory-Prepared Chars

Enter authors here: K. W. Bostick[1†], A. Z. Zimmerman[2], A. I. Goranov[3], S. Mitra[4], P. G. Hatcher[5] and A. S. Wozniak[6]

[1]Department of Geological Sciences, University of Florida, Gainesville, FL, United States.

[2]Department of Geological Sciences, University of Florida, Gainesville, FL, United States.

[3]Department of Chemistry and Biochemistry, Old Dominion University, Norfolk, VA, United States.

[4]Department of Geological Sciences, East Carolina University, Greenville, NC, United States.

[5]Department of Chemistry and Biochemistry, Old Dominion University, Norfolk, VA, United States.

[6]School of Marine Science and Policy, College of Earth, Ocean, and Environment, University of Delaware, Lewes, DE, United States

†Current Affiliation: Fugro USA Marine Inc., Seep Exploration

Corresponding author: Andrew R. Zimmerman (azimmer@ufl.edu)

Key Points:

- About half of pyrogenic dissolved organic carbon (pyDOC) was mineralized by soil microbes over 96 days
- PyDOC from chars made at lower temperatures and those pre-exposed to sunlight were biomineralized to greater extents
- Biomineralization caused relative increases in alkyl- and oxy-C, while aryl- (including condensed C) and low molecular weight-C decreased

Abstract

Pyrogenic dissolved organic matter (pyDOM) is known to be an important biogeochemical constituent of aquatic ecosystems and the carbon cycle. While our knowledge of pyDOM's production, composition, and photolability has been studied recently, we lack an understanding of potential microbial mineralization and transformation of pyDOM in the biogeosphere. Thus, leachates of oak charred at 400 and 650 °C, as well as their photodegraded counterparts, were incubated with a soil-extracted microbial consortium for up to 96 days. Over the incubation, significantly more carbon was biomineralized from the lower versus higher temperature char leachate (45% versus 37% lost, respectively). Further, the photodegraded leachates were biomineralized to significantly greater extents than their fresh non-photodegraded counterparts. Kinetic modeling identified the mineralizable pyDOC fractions to have half-lives of 9 to 13 days. Proton nuclear magnetic resonance spectroscopy indicated that the majority of this loss could be attributed to low molecular weight constituents of pyDOM (i.e., simple alcohols and acids). Further, quantification of benzenepolycarboxylic acid molecular markers indicated that condensed aromatic compounds in pyDOM were biomineralized to much less extents (4.4 and 10.1% decrease in yields of ΣBPCA-C over 66 days from Oak-400 and Oak-650 pyDOM, respectively), but most of this loss could be attributed to biomineralization of smaller condensed clusters (4 aromatic rings or less). These results highlight the contrasting bioavailability of different portions of pyDOM and the need to examine both to evaluate its role in aquatic heterotrophy and its environmental fate in the hydrogeosphere.

Plain Language Summary

Given the current increases in wildfire abundance and intensity, it is important to understand the fate of charred biomass in soils. As char is degraded in soils, it dissolves into porewaters where it then moves through the soil, into rivers, and ultimately the ocean. The current study strives to understand how microbial decomposition destroys or alters fire-derived dissolved organic carbon. To accomplish this, two chars were leached in water and were incubated with soil microbes. This study found that about half of the carbon in these leachates could be readily decomposed, i.e. converted back to carbon dioxide (with some variation with char leachate type). However, about a half of the leachate was resistant to microbial utilization. As such, one could

expect this remaining portion might be transported by rivers to the ocean, potentially influencing aquatic ecology and global carbon cycling.

1 Introduction

Fire-derived or 'pyrogenic' carbon (pyC) constitutes ~10% of soil and sediment organic C, on average (Bird et al., 1999; Cusack et al., 2012). While generally considered recalcitrant in the geosphere, pyrogenic organic matter (OM) can undergo dissolution aided by abiotic and biotic oxidation (Abiven et al., 2011; Cheng et al., 2006; Roebuck et al., 2017; Sorrenti et al., 2016), forming pyrogenic dissolved organic matter (pyDOM). This pyDOM leaches from soils and sediments where it enters aquatic C pools. A component of pyDOM, namely condensed aromatic carbon (ConAC), has been identified in wetlands (Ding et al., 2014), rivers (Ding et al., 2015), the ocean (Stubbins et al., 2012a; Ziolkowski & Druffel, 2010) and even glacial outflows (Stubbins et al., 2012b), using benzenepolycarboxylic acids (BPCA), molecular markers for condensed aromatic OM. Based on field and experimental leaching studies, up to 203 Tg of pyrogenic dissolved organic carbon (pyDOC) may enter aquatic systems annually (Bostick et al., 2018; Jaffé et al., 2013).

However, as a whole, this pyDOM is a heterogeneous mixture of low molecular weight compounds (e.g., acetate, methanol, and formate), oxygenated aliphatic hydrocarbons, thermally-altered biopolymers, and ConAC (Bostick et al., 2018; Fu et al., 2016; Norwood et al., 2013). But the absolute and relative amount of these components varies with pyDOM type. For example, the amount of pyDOM leached from chars decreases with parent char thermal maturity and is relatively greater from grass versus oaks parent chars (Bostick et al., 2018; Mukherjee & Zimmerman, 2013; Wozniak et al., 2020). Further, the proportion of ConAC in leached pyDOM generally increases with char thermal maturity (Bostick et al., 2018; Fu et al., 2016).

To understand the impacts of pyDOM on global carbon cycling, as well as its potential effects on aquatic heterotrophy, and even environmental and human health, the mobility and fate of pyDOM must be better understood. Several laboratory and field studies show that photochemical degradation is a major pyDOM mineralization and alteration pathway, particularly for its aromatic fraction (Bostick et al., 2020; Myers-Pigg et al., 2015; Stubbins et al., 2012a; Wagner et al., 2018; Ward et al., 2014). However, pyDOC, is also likely susceptible to biomineralization given that solid chars are biolabile to some degree (Baldock & Smernik,

2002; Bruun et al., 2012; Bruun et al., 2008; Zimmerman, 2010). In particular, pyDOM is rich in O-containing, aliphatic and low molecular weight compounds (the more soluble components of char, e.g., Bostick et al., 2018), which are likely to be bioavailable (e.g., Herlihy et al., 1987).

To date, studies that examined the biolability of pyDOM have been few and considered either only the condensed aromatic portion that is generally thought to be quite biorecalcitrant and difficult to metabolize (Kim et al., 2006; Spencer et al., 2015), or the non-condensed portion that has been shown to be readily biomineralizable (Norwood et al., 2013), but not both. In a microbial incubation study (Norwood et al., 2013), more than half the pyDOC from mesquite char leachates were mineralized within 1 month. In this same study, levoglucosan, derived from thermally altered carbohydrates, and free lignin phenols were almost completely lost in this timeframe. However, it should be kept in mind that these char leachates were made at 250 °C, and therefore relatively poor in ConAC, while most chars are prepared at higher temperatures (>500 °C).

Because BPCAs are commonly used to identify pyDOM in natural samples, and these compounds are derived only from their condensed aromatic OM portions, pyDOM is often represented as biorefractory (Wagner et al., 2018). However, environmental biodegradation of aromatic OM does occur. Using dioxygenase, manganese peroxidase, and monoxygenase enzymes, both lignolytic fungi and a wide variety of bacteria are able to oxidize small-cluster ConAC such as polycyclic aromatic hydrocarbons (PAH) into simple phenolic compounds (Bamforth & Singleton, 2005; Higuchi, 2004), though energy yields are low. Suggestion of the role of these processes in pyDOM degradation via microbial activity may also be found in the 20–80% increases in soil phenol oxidase activity in forest soils following burning events (Boerner & Brinkman, 2003). However, the breakdown of this aromatic fraction of pyDOM has not been specifically shown.

The ConAC portion, and to a lesser extent, the non-condensed portion of pyDOM has been shown to be highly photolabile, with 75-94% of ConAC and 5-8% of non-ConAC lost over five days of photoexposure (Bostick et al., 2020). However, photomineralization may not be able to account for the majority of pyDOM loss in the hydrosphere given that pyDOM spends only a small portion of its lifetime exposed to sunlight. For example, Amon and Benner (1996) calculated that, for Amazon River DOM, while photomineralization rates were seven times

greater than those of microbial DOC utilization, when integrated over the entire water column, microbial mineralization accounted for much more of the overall DOC loss.

It may be that biolability of pyDOM is increased by photoexposure. Several studies have shown that light exposure can increase the bioavailability of glacial, wetland, lacustrine, and marine DOM (Antony et al., 2018; Kieber et al., 1989; Lindell et al., 1995; Rossel et al., 2013), possibly due to the cleavage of macromolecules into smaller, more bioavailable units. Other studies found light to have little to no effect of photoexposure on DOM bioavailability (Amon & Benner, 1996; Andrews et al., 2000; Anesio et al., 2005; Benner & Biddanda, 1998). Still other studies suggested that photoexposure decreases biolability of DOM (Anesio et al., 1999; Keil & Kirchman, 1994; Tranvik & Kokalj, 1998). Given the characteristic photolability of pyDOM, its photoproducts may have unrecognized impacts on pyDOM microbial uptake and subsequent biomineralization.

In order to assess the influence of pyDOM on global C cycling, aquatic ecosystems, and to predict how these may be affected were aquatic pyDOM levels to increase, a better understanding of pyDOM biolability is needed. However, because pyDOM made at different temperatures varies widely in composition, particularly in regard to its condensed aromatic content, pyDOM derived from chars of a range of thermal maturities must be examined. Further, there is a need to simultaneously study the biolability of both condensed and non-condensed portions of pyDOM. Lastly, there is a need to understand the effects of photoexposure on pyDOM biolability. Therefore, in the current study, microbial incubations of fresh and photoirradiated leachates derived from chars of different thermal maturities were conducted. While pyDOC measurements were used to track the kinetics of overall biomineralization, BPCA analyses and spectroscopic methods were used to identify the biolability of various pyDOM components. We hypothesize the occurrence of two phases of pyDOM biomineralization, where small aliphatic compounds, particularly those with oxygen-containing functional groups are lost quickly, and condensed aromatic components are lost more slowly at rates controlled by cleavage of aromatic structures (e.g., da Cunha-Santino & Bianchini, 2002; Kiikkila et al., 2013; Qualls, 2005). Further, we hypothesize that photoexposure will increase the biolability of pyDOM. Testing these hypotheses, will better our understanding of pyDOM lability in the biogeosphere, as well as the molecular markers that are used to track pyDOM in the environment.

2 Materials and Methods

2.1 Production of Pyrogenic Parent Solids and their Leachates

Two chars were produced from laurel oak wood (*Quercus hemisphaerica,* roughly 0.5 x 0.5 x 4 cm pieces) by pyrolysis under flowing N_2 (held at peak temperatures of 400 and 650 °C for 3 h) and designated Oak-400 and Oak-650, respectively. Physiochemical data on these chars and their aqueous leachates have been reported previously (Bostick et al., 2018; Mukherjee & Zimmerman, 2013; Zimmerman, 2010).

A mortar, pestle, and sieving were used to achieve a semi-uniform 0.25–2.0 mm char particle size for leachate production. Using combusted glassware, approximately 5 g of each solid sample was added to 500 mL of MilliQ Nanopure water (18.1 MΩ) in 1 L amber-glass bottles. Following Bostick et al. (2018), the bottles were agitated on a platform shaker table at 80 rpm in the dark. After 50 hours, the leachates were pre-filtered through Fisherbrand glass fiber filters (1.0 mm particle retention), and subsequently filtered using a mixed cellulose ester (0.22 μm particle retention; Millipore GSWP) with the aid of a vacuum flask-based filtration manifold.

2.3 Photodegradation of pyDOM

A portion of each leachate was photoincubated for 5 days prior to microbial incubation. Aliquots of each leachate (80 mL) were transferred to 100 ml tubular quartz reaction vessels (~50 cm long, 3 cm outer diameter, 2 mm thick walls), sealed with Teflon caps, and placed horizontally in a photoincubation box with a ventilation fan to hold at room temperature (24 – 26 °C). Sunlight was simulated with four 40 watt, UV-A 340 nm lamps (Q-Lab Corporation) attached 27 cm from the quartz reaction vessels. These bulbs provided UV radiation approximating natural sunlight in the 295 to 365 nm wavelength region, which is the principal range for environmental photochemical reactions (Helms et al., 2008; Spencer et al., 2009). The irradiation energy at the water surface was estimated to be approximately 1.2 times terrestrial solar irradiation energy (i.e., 5 days in the photoincubation box simulates approximately 12 days of irradiation assuming 12 hours light per day, Bostick et al., 2020). Hereafter, photodegraded leachate samples are designated with ‘Photo’ as a prefix (e.g., Photo Oak-400) while non-irradiated samples are prefixed with ‘Fresh’ (e.g., Fresh Oak-650).

178 *2.4 Microbial Incubations*

179 Microbial inoculants were extracted from the organic-rich surface soil horizons of a pine-
180 dominated (*Pinus palustris*) upland forest in North-Central Florida (29°45'26.5" N, 82°12'16.2
181 W, Supplemental information Fig. S1). This site was selected because it is frequently subjected
182 to prescribed burns (burnt at least twice per decade, Johns, 2016). As a result, this soil microbial
183 consortia may regularly interact with pyrogenic OM. In addition, genetic sequencing of the
184 microbial taxa of this soil has been published (Khodadad et al., 2011).

185 After sieving (φ = -2 – 4) to remove roots and large detritus, the soil was homogenized
186 manually. Approximately 5 g soil subsets were mixed with 50 mL MilliQ Nanopure water (18.1
187 MΩ) in beakers over a warm plate (30°C), and gently agitated with magnetic stir bars for 45
188 minutes. After filtering with a 1.0 μm glass fiber filter (FisherBrand, G2), and centrifugation
189 (400 rpm, 10 minutes), the soil leachate supernatant was decanted. The remaining centrifugate
190 pellets were combined, added to 10 mL MilliQ Nanopure water, and used as the microbial
191 inoculant.

192 Aliquots of fresh and photoirradiated Oak-400 and Oak-650 leachates (50 mL) were diluted
193 to a uniform organic C concentration of 4.7 mg C L^{-1} and placed in 100 mL amber glass vials and
194 topped with gas-tight polytetrafluoroethylene septa. All sample vials received 100 μL of the
195 microbial inoculant. In addition, 1.0 mL aqueous nutrient solution consisting of 0.45 M
196 ammonium sulfate and 0.1 M monopotassium phosphate was added, i.e. an amount of N and P in
197 excess of that needed to mineralize all the organic C at Redfield stoichiometric ratios. Abiotic
198 controls were the Oak-400 and Oak-650 leachates + inoculant + nutrient mixtures poisoned with
199 5 μL of saturated mercuric chloride ($HgCl_2$) solution. Every sample vial was sparged with CO_2-
200 free air for 30 minutes (Airgas Zero Air, CGA-590) with a double needle assembly. Then, the
201 inoculated leachates were placed on a platform shaker table (60 rpm), in the dark, inside of a
202 Fisher Scientific Isotemp incubator kept at 28 ± 5 °C for a total of 96 days.

203

204 *2.5 Carbon Mineralization*

205 Mineralization of pyDOC was detected as *in situ* total inorganic carbon (TIC) in the
206 incubated solutions, and was measured on days 0, 2, 5, 10, 18, 26, 36, 46, 66, and 96 of the
207 incubations. Using a double needle assembly penetrating into the solution, this TIC was sparged
208 with CO_2 free air (Airgas Zero Air, CGA-590) and plumbed through a $AgNO_3$ solution and

209 detected with a CO_2 coulometer (UIC, Inc. 5017). This both removes all TIC from solution and
210 oxygenates the solution prior to further incubation. While no user-calibration is required for this
211 coulometer, the quality of these data was confirmed by routinely running known amounts of
212 $CaCO_3$ and $KHCO_3$ standards, which were acidified to produce CO_2. The precision of these
213 measurement was < 0.2% and the analytical detection limit was found to be 0.1 μg C. MilliQ
214 water blanks were also incubated and measured via coulometer to confirm the absence of gas
215 leakage.
216
217 *2.6 Dissolved Organic Carbon Analyses*
218 Aliquots (10 mL) of initial and incubated leachates (days 0, 10, and 66) were analyzed for
219 dissolved organic carbon (DOC) content on a Shimadzu TOC-VCSN with high-sensitivity Pt
220 catalyst after acidification to pH 2 (with trace metal grade HCl) and sparging for 2 min with N_2
221 to remove DIC. Standard curves were generated using potassium biphthalate solutions ranging
222 from 0.4 to 40 mg C L^{-1} (Sigma-Aldrich, >99.95%). These data were used to compare with
223 pyDOC mineralization measured via respired CO_2 and to normalize other chemical data (below)
224 to organic carbon content.
225
226 *2.7 BPCA Analyses*
227 BPCA compound are produced via the oxidation of condensed aromatic compounds,
228 including both 3 to 4-ring PAH compounds and large condensed aromatic clusters (Ziolkowski et
229 al., 2011). Here, we use changes in ΣBPCA-C (the sum of benzenetri-, benzenetetra,
230 benzenepenta- and benzenehexacarboxylic acids, notated as B3CA-C and B4CA-C, B5CA-C and
231 B6CA-C, respectively) as an indicator of biomineralization of all these BPCA-producing
232 compounds as a whole. Because B5CA and B6CA molecules are more robust markers of larger
233 condensed aromatic clusters, and given B3CAs and B4CAs have been found to be produced by
234 non-pyrogenic OM sources (Bostick et al., 2018, Kappenberg et al., 2016), ConAC content was
235 calculated here as the carbon found in B5CA-C and B6CA-C only, multiplied by a factor of 7.04,
236 derived from experimentally-derived graphene oxide oxidation efficiency (Bostick et al., 2018).
237 Trends in the varying proportions of the BPCA compounds are represented here by a
238 benzenepolycarboxylic acid aromatic condensation index (BACon-index, i.e., the average
239 number of carboxyl substitutions among the BPCAs produced).This index has been used

previously by Bostick et al. (2018 and 2020) and Ziolkowski et al. (2010) as a relative indicator of condensed aromatic cluster size.

Analyses of BPCA were based upon Dittmar (2008) and are described in detail in Bostick et al. (2018). Briefly, 40 mL aliquots of initial and incubated (days 10 and 66) leachates were acidified to pH 2, loaded onto Agilent PPL cartridges (3 mL, 100 mg) and eluted with 10 mL methanol. After drying, the eluents and approximately 0.5 mL concentrated nitric acid (65%) were flame-sealed into 1.5 mL glass ampoules, placed in Parr pressure bombs, and heated to 170 °C for 9 hours. Digested products were concentrated and transferred into Teflon septa-topped vials. BPCA compounds were separated and detected via high performance liquid chromatography (HPLC, Shimadzu LC-20 Prominence Series) equipped with a C_{18} column (3.5 µm, 2.1 × 150 mm, Waters Sunfire) and a diode array detector (DAD) (Surveyor, Thermo-Scientific, SPD-M20A) using a buffered binary gradient (i.e., H_2O and methanol-based) program.

2.8 ^1H Nuclear Magnetic Resonance Spectroscopy

Proton nuclear magnetic resonance (NMR) spectroscopy was used to examine changes in organic functional group distributions of the leachates due to microbial utilization. Initial and 10 day microbially-incubated leachates were spiked with sodium 2,2,3,3-tetradeutero-3-trimethylsilylpropanoate (TMSP, Acros Organics, 98 % D) to obtain a 1 µM TMSP final concentration, and diluted with deuterated water (D_2O, Acros Organics, 100% D) at a volumetric ratio of 9:1 (i.e., H_2O:D_2O). NMR spectra of these deuterated pyDOM solutions were obtained on a Bruker Biospin AVANCE III 400 MHz NMR spectrometer, fitted with a Double Resonance Broadband Inverse probe, at Old Dominion University's College of Sciences Major Instrumentation Cluster (COSMIC) facility. One-dimensional ^1H spectra were obtained using a 4 s relaxation delay, 10,000 scans, and a pulse program performing Perfect-Echo-WATERGATE water suppression (Adams et al., 2013; Whitty et al.), following previous studies (e.g., Wozniak et al., 2013). To correct for matrix effects, a $HgCl_2$-poisoned blank amended with the microbial inoculate and nutrients, was filtered using a 0.2 µm membrane filter, and used as a procedural blank which was subtracted from all spectra by normalizing the data to the TMSP peak ($\delta \approx$ -0.02 ppm). Spectra were then integrated over specific chemical shift regions that are characteristic of ^1H chemical environments.

Spectra were divided into regions that represent different functional groups as follows. The region between 0.60 and 1.80 ppm (termed 'Alkyl-C') includes signals from methyl-H (0.6 – 1.0 ppm), methylene-H (1.0 – 1.4 ppm), and H in alkyl groups that have heteroatoms bound to a beta C (HC-C-CX, where X is O, N, S, etc., 1.4 – 1.8 ppm). The regions between 1.8 – 4.4 ppm and 8.3 – 10.0 ppm (termed 'Oxygenated-C') includes signal from carbonyl and carboxyl functional groups, H bound to C bound to N or S (HC-N or HC-S, 1.8 – 3.2 ppm), carbohydrate and alcohol groups (HC-OR, 3.2 – 4.4 ppm) and aldehydes (O=CH, 8.3 – 10.0 ppm). The region between 6.5 and 8.3 ppm (termed 'Aryl-C') corresponds to H attached to aromatic C. Lastly, H in acetic acid / acetate (1.9 – 2.1 ppm), methanol (3.2 – 3.4 ppm) and formic acid (8.1 – 8.3 ppm) appeared in some spectra as sharp singlet peaks indicative of pure compounds. Signal corresponding to these three regions was summed and reported as 'low molecular weight-C' (LMW-C) compounds, and subtracted from the alkyl-C, oxygenated-C, or aryl-C regions in which their chemical shifts occurred. Not considered, is ^{1}H signal between 4.4 and 5.0 ppm, which includes some amine and ester H, as the resonances in this region are attenuated by the water suppression pulses.

Spectral signals in each chemical shift region were integrated using Bruker Topspin software. For comparison of the NMR data with other quantitative data (e.g., TOC measurements), the ^{1}H NMR spectral assignments were converted to a C-basis following Decesari et al. (2007) by dividing each integrated area by H/C ratios typical of the ^{1}H environments in that chemical shift region. The relative contribution of each chemical shift region was then calculated as the C-basis area divided by the sum of all C-basis areas.

2.9 Replication and Data Analysis

All leachate types were incubated in quadruplicate until day 10, when one of each replicate was harvested for BPCA-C analysis and thereupon incubated in triplicate. Significant differences among pyDOC loss amounts and rates (time versus DOC concentration slopes) were compared for the 'early' (days 0 – 5) and 'late' (days 46 – 96) incubation period using Microsoft Excel's t-test function ($\alpha = 0.05$ level). Both TIC and DOC analyses were replicated 5 times and additional analyses were run if coefficients of variation exceeded 5%. While analyses of BPCA were not replicated for this study, previous analyses of similar samples in our laboratory yielded analytical variation of BPCA-C ranging 7.0 – 33.3% (20.8 ± 8.1 for average ± std. dev., Bostick et al., 2018).

A first-order exponential decay equation was used to model DOC mineralization kinetics for each leachate such that:

$$\mathbf{C_t} = \boldsymbol{C_{m_0}}\mathbf{e^{-kt}} + \mathbf{C_{nm}} \quad \text{(Eq. 1)}$$

where C_t is the amount of total pyDOC remaining at time t, C_{m0} is the initial concentration of mineralizable pyDOC, C_{nm} is the amount of non-mineralized carbon (defined as the carbon remaining after 96 days), and k is the apparent first order biomineralization rate constant for the degradable portion of pyDOC. The non-linear regression tool available on SigmaPlot 14 was used to fit equation 1 to the incubation data.

3 Results and Discussion

3.1 Biomineralization of pyDOC

All measurements of C mineralization calculated using cumulative evolved DIC were within 2% of those calculated using DOC loss at the end of each incubation. The extent and rate of fresh pyDOC mineralization was significantly greater in microbial versus abiotic (control) incubations ($p < 0.01$) and varied with parent char temperature (Fig. 1). Poisoned controls of Oak-400 and Oak-650 leachates only lost 8 ± 1% of its DOC over 96 days of incubation, giving some estimate of the extent of abiotic oxidation that may occur in the environment.

Over the 96-day microbial incubation, significantly more fresh pyDOC was lost from the lower temperature char leachate (45 ± 2% loss from Fresh Oak-400) than from the higher temperature char leachate (37 ± 3% loss from Fresh Oak-650, $p = 0.02$). These results were expected as Oak-400 char and its leachates are known to contain higher proportions of compounds that are considered to be readily bioavailable (i.e. rich in carbohydrates and LMW compounds, Bostick et al., 2018). Correspondingly, the extent of biomineralization reported here is less than that reported for 250 °C mesquite char leachate over 37 days (i.e. 60% C loss, Norwood et al., 2013). While the rate of pyDOC loss from the Oak-400 leachate was significantly greater than that from the Oak-650 leachate in the early portion of the incubation (1.8 times greater during the first 5 days), late incubation (between days 46 and 96) loss rates from fresh Oak-400 and Oak-650 were not statistically different from each other or from those of the poisoned controls. This supports the postulation of an essentially non-biomineralizable portion of the pyDOM, assumed in the pyDOC degradation model (see below).

The photodegraded leachates from both chars biomineralized at significantly higher rates than fresh char leachates over the first 5 days (by about 1.5 times; Fig. 1). By the end of the incubation (day 96), pyDOC loss from photodegraded leachates was significantly greater than from their fresh leachate counterparts (by 10.6%, on average). This phenomenon has been observed with natural DOM whereby photoexposure increased the microbial mineralization of glacier DOM by roughly 60% over 35 days (Antony et al., 2018) and photoexposure of dissolved humic substances caused a 1.5 to 6-fold increase in bacterial production (Moran & Zepp, 1997).

3.2 Biodegradation of Condensed OM in Fresh Leachates

Condensed aromatic components of pyDOM were biomineralized to a much lesser extent than other constituents of pyDOM. Approximately 4.4 and 10.1% of ΣBPCA-C was lost from fresh Oak-400 and Oak-650 pyDOM, respectively, over 66 days (Fig. 2). These losses were significantly greater than the 2% losses of ΣBPCA-C from both abiotic incubations over the same period ($p = 0.3$), indicating that degradation of condensed OM was microbial mediated. These low rates of BPCA-yielding OM utilization are on the order of that observed for condensed tannins (0.1 – 11.0% over 4 weeks, Nierop et al., 2006), but lower than losses of PAH, i.e. 19-53% over 15 weeks in a simulated sandy soil with white rot fungi (Wolter et al., 1997).

BACon-values of both fresh Oak-400 and fresh Oak-650 leachates were initially quite similar (4.0 ± 0.1). After 66 days of microbial incubation, the BACon-values of these fresh leachates had increased by 0.02 and 0.1, respectively, indicating that the average size of aromatic clusters in pyDOM increased slightly with microbial incubation (Fig. 2). This is also illustrated by the greater reduction in yields of B3CA+B4CA-C (5.1 and 15.6% loss from Oak-400 and Oak-650 leachates, respectively, Fig. S2), compared to that of B5CA+B6CA-C (2.2 and 1.4%, respectively). The former are derived from all condensed units (3 aromatic rings and larger) whereas the latter are only produced by condensed clusters of > 4 aromatic rings (Bostick et al., 2018; Ziolkowski et al., 2011).

These molecular shifts in BPCA-yield can be attributed to mineralization of lower molecular weight condensed compounds, i.e. those of smaller cluster size, in preference to larger ones. They explain the greater loss of ΣBPCA-C from Oak-400 versus Oak-650 leachates as the former are richer in these smaller condensed compounds. Biolability has previously been shown

to scale with the number of aromatic rings in a compound. For example, one study showed that while 2-ring PAHs have half-lives of 10 days in soil, 5-ring PAHs have half-lives that can exceed 200 days (McGinnis et al., 1988; Sims et al., 1988). A potential but rather unlikely alternative is that large clusters of condensed OM were formed during the incubations via microbial or abiotic cyclopolymerization reactions (i.e., similar to those observed under sunlit Fenton conditions by Waggoner et al., 2015). For example, one study detected *in situ* biological formation of BPCA-yielding compounds in soils (Glaser & Knorr, 2008). Another study found that the fungus *Aspergillus niger* yielded BPCA compounds, particularly BP6CAs (Brodowski et al., 2005).

The 1.4 – 2.2 % loss of larger aromatic OM over the 66-day incubation (ConAC, calculated using only B5CA and B6CA markers) was similar to the 2.0 – 2.4% loss of ConAC from abiotic controls (Fig. 3). Thus, a large portion of the losses from microbial incubations can be attributed to abiotic oxidation or even, potentially, flocculation of ConAC. These results indicate that, under these experimental conditions, pyDOM with the highest degree of condensation (e.g., most aromatic rings) was nearly wholly biorecalcitrant. These results align with those of Kim et al. (2006) in which very little pyrogenic stream DOM, detected as hydrogen-deficient molecules with low H:C ratios, was metabolized in biofilm reactors.

3.3 Biodegradation of Photo-treated Leachate ConAC

As has been reported previously with these same char leachates (Bostick et al., 2020), about 10 – 20% DOC was lost over 5 days of photoincubation while the ΣBPCA-C yield decreased by 61 to 73%. Condensed pyDOC of larger cluster size was most susceptible to photodegradation as indicated by a 73-95% decrease in yield of B5- and B6CA compounds and an average decrease in BACon values from 4.0 ± 0.1 to 3.6 ± 0.1 (Fig. 2). During the 66 days of microbial incubation, 10.1 and 7.7% of ΣBPCA-C was lost from the photodegraded Oak-400 and Oak-650 leachates, respectively, which is significantly more (by about 5 times) than was lost from their fresh leachate counterparts ($p = 0.04$, Fig. 2). BACon-values of photodegraded Oak-400 and Oak-650 leachate increased by 0.11 and 0.07, respectively, indicating that the average size of condensed aromatic clusters in pyDOM increased slightly with microbial incubation. These data further support the conclusion that aromatic compounds with fewer rings were more biolabile than larger ones.

The greater mineralization of pre-photoexposed pyDOM (compared to fresh pyDOM) can be explained by its lower condensed C (ΣBPCA-C and ConAC) content. Further, the greater mineralization of the condensed portion in pre-photoexposed pyDOM can be explained by its relatively greater proportion of smaller sized aromatic clusters. Another possibility is that 'photopriming' occurred, whereby photoexposure created labile compounds that stimulated the production of microbial enzymes, leading to the enhanced biomineralization of more refractory components. Priming of solid pyrogenic matter due to the presence of more labile non-pyrogenic organic components has been observed previously (Zimmerman & Ouyang, 2019; Zimmerman et al., 2011) and photoexposure has been found to stimulate the biomineralization of otherwise refractory leaf litter lignin (Austin et al., 2016; Lin et al., 2018).

3.4 Functional Group Composition of Fresh and Degraded pyDOM

After 10 days of microbial incubation of pyDOM, carbon present in low molecular weight (LMW) organic components (e.g, formate, formic acid, methanol, acetate, and acetic acid), which initially constituted 20 – 50% of pyDOC, were almost entirely consumed (Fig. 4 and supplementary information Table S2). Methanol and formate was likely mineralized by methylotrophic bacteria and/or methylotrophic fungi, the only microbes known to consume C1 constituents of DOM (Chistoserdova & Kalyuzhnaya, 2018; Chistoserdova et al., 2003; Kolb & Stacheter, 2013). These methylotrophs have previously been identified in the soil microbiome used in this study (e.g., methylococcaceae and methylobacteriaceae, Khodadad et al., 2011). Formic and acetic acids have been previously demonstrated to be readily bioavailable to heterotrophic bacteria (i.e., turnover rate constants ~0.2 h, Herlihy et al., 1987). In addition to these LMW constituents, there was a 25 – 67% relative decrease in aryl-C over the same period in all leachates, indicating a sizable decrease in the pyDOM's aromatic content. This aromatic pyDOM could have been degraded by both α-and γ-Proteobacteria, which are known to degrade lignin using lignin peroxidase and manganese peroxidase enzymes (Tian et al., 2014). These taxa have also previously been identified in the microbial consortium used in this study (Khodadad et al., 2011). The proportion of aryl-C losses were considerably greater than those of ΣBPCA-C suggesting that much of the aryl-C in these samples contains fewer than 3 aromatic rings and provides further evidence for a inverse relationship between biolability and number of aromatic rings in a compound.

After 10 days of microbial incubation, the remaining pyDOC was mainly composed of oxygenated-C and alkyl-C (e.g., methyl-C, methylene-C, and aliphatic compounds bonded with O, N, and S) with smaller portions of vinylic-C (supplementary information Table S2). It is likely that these groups represent thermally altered cellulose components, which require extensive enzymatic degradation before they can be utilized (Payne et al., 2015).

Compared to the fresh pyDOM leachates, photodegraded leachates were relatively depleted in aryl-C and enriched in oxygenated-C components (Fig. 4). Whereas the LMW component of Oak-400 decreased with photoexposure, that of Oak-650 increased. These results are consistent with previous findings that photodegradation of pyDOM converts condensed aromatic units (which were of more relative abundance in Oak-650 pyDOM) into smaller aromatic and aliphatic compounds (Bostick et al., 2020).

Biodegradation of the photodegraded pyDOM samples yielded patterns of relative functional group change similar to those of fresh pyDOM samples, namely: nearly total loss of LMW-C, decreased aryl-C, increased oxygenated- and alkyl-C. Thus, it is likely that the photodegradation increased the rate and extent of pyDOC biomineralization by breaking large compounds, including condensed aromatics, into LMW and other more easily metabolizable components. This is supported by previous studies which show rapid utilization of small compounds such as LMW organic acids produced by photolysis of even recalcitrant DOM (Brinkmann et al., 2003; Wetzel et al., 1995).

3.5 pyDOM Biomineralization Kinetics and Mechanisms

Longer-term estimates of pyDOC bioavailability are needed to understand the potential export of pyrogenic C from land to ocean, information needed for global pyC cycling models. The majority of biomineralization occurred early in the incubations with about 80% of all pyDOC loss occurring in the first 26 days of the biotic incubations (and 20% lost in the remaining 70 d). As pointed out above, rates of mineralization in this later incubation period were low (~0.1% daily loss), and not significantly different from the abiotic control. This supports the assumption, for the purpose of modeling, of two pyDOM components: 1) a biolabile portion that is readily biomineralizable, and 2) a pyDOM portion that does not biomineralize under the experimental conditions (i.e., is mineralized at rates indistinguishable from those of the abiotic controls).

455 The loss of the mineralizable portion of pyDOC was successfully simulated using a single-
456 component exponential decay equation (Eq. 1, all r^2 values ≥ 0.98, Table 1). A two-component
457 decay equation did not simulate the data substantially better (i.e., did not yield significantly
458 higher r^2 values). This suggests that, compared to solid pyrogenic solids, whose degradation
459 kinetics simulation commonly requires a 2-component model (e.g., Fang et al., 2014;
460 Zimmerman, 2010), the dissolved pyC may be of more uniform availability to microbes.
461 Using the single-component model, the biomineralizable fraction of fresh pyDOM was
462 calculated to have experimental half-lives of approximately 12−13 days and accounted for
463 approximately 45% and 37% of the total DOC in Fresh Oak-400 and Oak-650 leachate,
464 respectively. These fractions roughly corresponded to the estimated amount of pyDOC initially
465 present as LMW-C (i.e., 50% and 27%, respectively), the component lost to the greatest extend
466 during microbial incubation, as determined by ^{1}H-NMR spectroscopy data. Thus, the majority of
467 C loss could be attributed to LMW-C mineralization. The half-life of this biomineralizable
468 fraction is slightly longer than the half-lives of other non-condensed components of pyDOM
469 from lightly charred biomass. For example, levoglucosan and free lignin phenols were shown to
470 have half-lives of 4 and 5 days, respectively (Norwood et al., 2013). These shorter half-lived are
471 likely due to the molecular-level lability of these components rather than their lower thermal
472 maturity, as the bioavailable portions of the 400 and 650 ºC char pyDOM were found to have
473 similar half-lives (Tab. 1).
474 The biorecalcitrant pyDOM accounted for approximately 55% and 63% of the total pyDOC
475 in Fresh Oak-400 and Oak-650 leachates, respectively. Given that ConAC was largely resistant
476 to degradation (only ~2% loss over 66 days), it is clear that ConAC constitutes a portion of this
477 recalcitrant pyDOM fraction. However, given the amounts present in pyDOM, ConAC can only
478 account for 5-25% this biorecalcitrant fraction. Thus, the remaining 75-95% of this
479 biorecalcitrant fraction must be made up of small aromatic compounds (< 4 rings) and non-
480 aromatic compounds, the latter of which, according to the ^{1}H-NMR data, was primarily
481 composed of oxygenated and alkylated carbon. While oxygenated and alkylated forms of
482 compounds are not generally thought to be refractory, it is possible that the presence of phenolic
483 or condensed compounds inhibited microbial enzyme synthesis or activity, decreasing microbial
484 utilization of this otherwise biolabile DOM. This may be similar to the inhibitory effect of humic
485 and aromatic substances on labile aquatic DOM mineralization observed by Mann et al. (2013),

Tejirian and Xu (2011), and Backes et al. (1993) in blackwater settings. Some pyDOM compounds may also become microbial inaccessible through their complexation with metals or colloids (Marschner & Kalbitz, 2003). More specifically, oxygenated and alkyl DOM have been shown to chemically bind with DOM components (Guggenberger et al., 1994; Jandl & Sollins, 1997), which can shield them from enzymatic attack. Thus, it may be that interactions between different pyDOM components resulted in their inaccessibility to microbial mineralization, as opposed to their intrinsic chemical recalcitrance.

The biomineralizable fraction of photodegraded Oak-400 and Oak-650 leachates degraded only slightly faster than their fresh counterparts (i.e., experimental $t_{1/2}$ of approximately 9 and 11 days, respectively). This mineralizable fraction represented approximately 48% and 41% of Photo Oak-400 and Photo Oak-650 leachates, respectively. Unlike the fresh leachates, the amount of the biomineralizable component in photo-treated samples was somewhat greater than the amount of pyDOC initially present as LMW-C (i.e., about 20 and 37% in Photo Oak-400 and Oak-650, respectively), as estimated from ^{1}H-NMR spectroscopy data. Thus, unlike for the fresh leachates, there must have been considerable C mineralization in the photo-treated leachates (particularly that of Photo Oak-400) that were not attributable to LMW compounds. Using a C mass balance calculation approach, one study indicated that, in addition to LMW compound production, higher molecular weight compounds might also be altered by light exposure so that their biolability is increased (Miller & Moran, 1997). Thus, the term ‘photolabilization’ could be broadly applied to the experimental results. As discussed above, photopriming may also have occurred but it cannot be confirmed with the current data.

The biorecalcitrant portion accounted for approximately 52% and 59% of the total pyDOC in Photo Oak-400 and Oak-650 leachates, respectively. However, ConAC could, at most, only account for about 3% of this biorecalcitrant fraction as the majority of ConAC was lost during photodegradation. These proportions are somewhat less than those noted above for non-photoexposed pyDOC and further suggest some mechanism, such as humic or metal interaction, whereby compounds thought of as biolabile were shielded from mineralization. In any case, photoexposure did not increase the recalcitrant of pyDOM, as has been previously observed through the interaction of sunlight, humic matter, and algae-derived DOM (Tranvik & Kokalj, 1998).

4 Conclusions: Implications and Environmental Significance

Does biomineralization of DOM derived from fire-altered biomass differ substantially from biomineralization of other natural DOM sources? In terms of biodegradability, about 40-50% of the pyDOC in this study was lost over 90 d. This generally falls between the larger proportion of fresh biomass leachate that is commonly lost in microbial incubation experiments and the much smaller portion of soil DOM that has been shown to be biomineralizable over similar time periods. For example, 56 – 84% of algal DOC (Lee et al., 2016), 35 – 95% of forest throughfall DOC (Qualls & Haines, 1992) and 61 – 93% of leaf litter and straw leachate DOC (Kalbitz et al., 2003a; Strauss & Lamberti, 2002) was lost over 60, 134, and 24 d of incubation, respectively. In contrast, mineralization of DOC from mineral soils ranged from 1 to 20% over similar periods (e.g., Qualls & Haines, 1992; Schwesig et al., 2003; Vujinović et al., 2019). Thus, the pyrolysis of biomass can be likened to soil processes such as OM decomposition and humification which make the DOM derived from soil OM progressively less biodegradable (Kalbitz et al., 2003a). As with soil DOM, pyDOM biodegradability is also likely closely related to its chemical properties, decreasing with aromaticity, degree of condensation (Kalbitz et al., 2003a; Kalbitz et al., 2003b), and generally increasing with the availability of LMW compounds (van Hees et al., 2005).

The 40-50% of the pyDOC found to be readily bioavailable in this study might be expected to be lost within the soil vadose zone, preventing its export by rivers to the ocean. Exposure to sunlight, i.e. photolysis, will further expedite pyC biomineralization, as it increases the bioavailability of pyDOM, mainly by converting condensed pyDOM to non-condensed compounds. About 50-60% of pyDOC (whether fresh or photodegraded or from low or high temperature parent solids) resisted biomineralization over the course of the 14 week experiment. Surprisingly, this refractory portion was not primarily composed of condensed OM. In a soil matrix, this pyDOM may be protected from biomineralization to even greater extents, as compounds are adsorbed to clay minerals, or interact with natural humic matter. On the other hand, pyDOM may be degraded to a larger extent in the soil environment due to more favorable conditions there because of a wider microbial consortia, or the occurrence of priming by a more labile soil DOM component.

These caveats aside, the results of this study can be viewed in the context of a series of studies that used the same set of laboratory-produced chars and char leachates. These studies

548 followed pyDOM from its production (Bostick et al. 2017) to its photo- (Bostick et al., 2020;
549 Goranov et al., Accepted) and bio-degradation (this study) and can be generalized in a single
550 figure (Fig. 5). An overall conclusion is that, while the aromatic fraction (10 to 21% of the
551 pyDOC initially leached) can be rapidly lost to photomineralization (about half the aryl C and up
552 to 95% of the ConAC fraction lost over 5 days), and a LMW fraction is likely to be lost to
553 biomineralization (40-50% of the pyDOC), it is largely the alkyl and O-functionalized C fraction
554 that is most likely to escape immediate mineralization and be exported to the ocean.
555 The majority of past pyDOM cycling studies have used BPCA and high resolution mass
556 spectroscopic analyses of environmental samples (e.g., Ding et al., 2013; Dittmar et al., 2012;
557 Kaal et al., 2016; Stubbins et al., 2012a; Ward et al., 2017; Ziolkowski et al., 2011).
558 Consequently, most of our prior knowledge of pyDOM biodegradation has focused only on the
559 condensed portion of pyDOM. The results of this study emphasize the need to understand
560 mineralization rates of bulk pyDOC along with the condensed portion, as there are important
561 differences, interactions and transfers between these pools. Unfortunately, we do not yet have a
562 way of distinguishing pyrogenic from non-pyogenic sources of this fraction in natural samples. It
563 is hoped that tracers (biomarker compounds) may be discovered so that pyDOC can be followed
564 through the environment and its influence on global C cycling modeled. However, results of this
565 study can already help to refine estimates of pyrogenic C contributions to global C cycling
566 budgets and models.
567 Both the increased application of biochar to soils and frequency of wildfires and prescribed
568 burning may increase the delivery of pyDOM to aquatic systems. The expected increase in
569 biolabile pyDOM may expedite non-pyrogenic DOM mineralization through priming, while
570 other pyDOM components may bind to both organic and metallic contaminants and assist in their
571 transport through the environment. Further studies are needed that explore; 1) molecular-level
572 changes in pyDOM during microbial utilization, perhaps using high resolution mass
573 spectrometry, 2) interactions between pyDOM and non-pyrogenic DOM that may either increase
574 or decrease their bioutilization, and 3) changes in pyDOM composition that may be used to
575 indicate the degree to which pyDOM is altered by microbial processes in natural systems.
576
577 **Acknowledgements and Data Availability**

This work was funded by the U.S. National Science Foundation - Geobiology and Low-Temperature Geochemistry Program (EAR-1451367). We thank Jason Curtis for his help with colorimetric analyses and the ODU COSMIC facility for assistance with ^{1}H NMR measurements. Lastly, we thank UF Geological Science department engineer Dow Van Arnam for helping with construction of incubation apparatus. Additional data and figures related to this article is available in the accompanying Supplemental Information. Raw data can be downloaded from https://figshare.com/ (file to be added).

References

Abiven, S., P. Hengartner, M. P. W. Schneider, N. Singh, & M. W. I. Schmidt (2011). Pyrogenic carbon soluble fraction is larger and more aromatic in aged charcoal than in fresh charcoal. *Soil Biology & Biochemistry, 43(7)*, 1615-1617. https://doi.org/10.1016/j.soilbio.2011.03.027.

Adams, R. W., C. M. Holroyd, J. A. Aguilar, M. Nilsson, & G. A. Morris (2013). "Perfecting" WATERGATE: clean proton NMR spectra from aqueous solution. *Chemical Communications, 49(4)*, 358-360. https://doi.org/10.1039/C2CC37579F.

Amon, M. W., & R. Benner (1996). Photochemical and microbial consumption of dissolved organic carbon and dissolved oxygen in the Amazon River system. *Geochimica et Cosmochimica Acta, 60(10)*, 1783-1792. https://doi.org/10.1016/0016-7037(96)00055-5.

Andrews, S. S., S. Caron, & O. C. Zafiriou (2000). Photochemical oxygen consumption in marinewaters. A major sink for colored dissolved organic matter? *Limnology and Oceanography, 45*, 267-277. https://doi.org/10.4319/lo.2000.45.2.0267.

Anesio, A. M., C. M. T. Denward, L. J. Tranvik, & W. Graneli (1999). Decreased bacterial growth on vascular plant detritus due to photochemical modification. *Aquatic Microbial Ecology, 17*, 159-165. http://DOI:10.3354/ame017159

Anesio, A. M., W. Granéli, G. R. Aiken, D. J. Kieber, & K. Mopper (2005). Effect of Humic Substance Photodegradation on Bacterial Growth and Respiration in Lake Water. *Applied and Environmental Microbiology, 71(10)*, 6267. https://doi.org/10.1128/AEM.71.10.6267-6275.2005.

608 Antony, R., A. S. Willoughby, A. M. Grannas, V. Catanzano, R. L. Sleighter, M. Thamban, & P.
609 G. Hatcher (2018). Photo-biochemical transformation of dissolved organic matter on the
610 surface of the coastal East Antarctic ice sheet. *Biogeochemistry, 141*, 229-247.
611 https://doi.org/10.1007/s10533-018-0516-0.
612 Austin, A. T., M. S. Mendez, & C. L. Ballare (2016). Photodegradation alleviates the lignin
613 bottleneck for carbon turnover in terrestrial ecosystems. *Proceedings of the National*
614 *Academy of Sciences of the United States of America, 113(16)*, 4392-4397.
615 https://doi.org/10.1073/pnas.1516157113.
616 Backes, W. L., G. Cawley, r. C. S. Eye, M. Means, K. M. Causey, & W. J. Canady (1993).
617 Aromatic hydrocarbon binding to cytochrome P450 and other enzyme binding sites: are
618 hydrophobic compounds drawn into the active site or pushed from the aqueous phase?
619 *Archives of Biochemistry and Biophysics, 304(1)*, 27-37.
620 https://doi.org/10.1006/abbi.1993.1317.
621 Baldock, J. A., & R. J. Smernik (2002). Chemical composition and bioavailability of thermally,
622 altered *Pinus resinosa* (Red Pine) wood. *Organic Geochemistry, 33(9)*, 1093-1109.
623 https://doi.org/10.1016/S0146-6380(02)00062-1.
624 Bamforth, S. M., & I. Singleton (2005). Bioremediation of polycyclic aromatic hydrocarbons:
625 current knowledge and future directions. *Journal of Chemical Technology and*
626 *Biotechnology, 80(7)*, 723-736. https://doi.org/10.1002/jctb.1276.
627 Benner, R., & B. Biddanda (1998). Photochemical transformations of surface and deep marine
628 dissolved organic matter: Effects on bacterial growth. *Limnology and Oceanography, 43*,
629 1373-1378. https://orcid.org/0000-0002-1238-2777.
630 Bird, M. I., C. Moyo, E. M. Veenendaal, J. Lloyd, & P. Frost (1999). Stability of elemental
631 carbon in a savanna soil. *Global Biogeochemical Cycles, 13(4)*, 923-932.
632 https://doi.org/10.1029/1999GB900067.
633 Boerner, R. E. J., & J. A. Brinkman (2003). Fire frequency and soil enzyme activity in southern
634 Ohio oak-hickory forests. *Applied Soil Ecology, 23(2)*, 137-146.
635 https://doi.org/10.1016/S0929-1393(03)00022-2.
636 Bostick, K., A. R. Zimmerman, A. Goranov, S. Mitra, P. G. Hatcher, & A. S. Wozniak (2020).
637 Photolability of pyrogenic dissolved organic matter from a thermal series of laboratory-

prepared chars. *Science of The Total Environment, 724*, 1-9. https://doi.org/10.1016/j.scitotenv.2020.138198.

Bostick, K. W., A. R. Zimmerman, A. S. Wozniak, S. Mitra, & P. G. Hatcher (2018). Production and composition of pyrogenic dissolved organic matter from a logical series of laboratory-generated chars. *Frontiers in Earth Science, 6*, 1-14. https://doi.org/10.3389/feart.2018.00043.

Brinkmann, T., P. Horsch, D. Sartorius, & F. H. Frimmel (2003). Photoformation of low-molecular-weight organic acids from brown water dissolved organic matter. *Environmental Science & Technology, 37(18)*, 4190-4198. https://doi.org/10.1021/es0263339.

Brodowski, S., A. Rodionov, L. Haumaier, B. Glaser, & W. Amelung (2005). Revised black carbon assessment using benzene polycarboxylic acids. *Organic Geochemistry, 36(9)*, 1299-1310. https://doi.org/10.1016/j.orggeochem.2005.03.011.

Bruun, E. W., P. Ambus, H. Egsgaard, & H. Hauggaard-Nielsen (2012). Effects of slow and fast pyrolysis biochar on soil C and N turnover dynamics. *Soil Biology & Biochemistry, 46*, 73-79. https://doi.org/10.1016/j.soilbio.2011.11.019.

Bruun, S., E. S. Jensen, & L. S. Jensen (2008). Microbial mineralization and assimilation of black carbon: Dependency on degree of thermal alteration. *Organic Geochemistry, 39(7)*, 839-845. https://doi.org/10.1016/j.orggeochem.2008.04.020.

Cheng, C. H., J. Lehmann, J. E. Thies, S. D. Burton, & M. H. Engelhard (2006). Oxidation of black carbon by biotic and abiotic processes. *Organic Geochemistry, 37(11)*, 1477-1488. https://doi.org/10.1016/j.orggeochem.2006.06.022.

Chistoserdova, L., & M. G. Kalyuzhnaya (2018). Current trends in methylotrophy. *Trends in Microbiology, 1*, 703-714. https://doi.org/10.1016/j.tim.2018.01.011.

Chistoserdova, L., S.-W. Chen, A. Lapidus, & M. E. Lidstrom (2003). Methylotrophy in Methylobacterium extorquens AM1 from a genomic point of view. *Journal of Bacteriology, 185(10)*, 2980-2987. http://doi:10.1128/jb.185.10.2980-2987.2003.

Cusack, D. F., O. A. Chadwick, W. C. Hockaday, & P. M. Vitousek (2012). Mineralogical controls on soil black carbon preservation. *Global Biogeochemical Cycles, 26*, 1-10. https://doi.org/10.1029/2011GB004109.

667 da Cunha-Santino, M. B., & I. Bianchini (2002). Humic substance mineralization in a tropical
668 oxbow lake (Sao Paulo, Brazil). *Hydrobiologia, 468(1-3)*, 33-43.
669 http://DOI:10.1023/A:1015214005279.
670 Decesari, S., M. Mircea, F. Cavalli, S. Fuzzi, F. Moretti, E. Tagliavini, & M. C. Facchini (2007).
671 Source attribution of water-soluble organic aerosol by nuclear magnetic resonance
672 spectroscopy. *Environmental Science & Technology, 41(7)*, 2479-2484.
673 https://doi.org/10.1021/es0617111.
674 Ding, Y., Y. Yamashita, W. K. Dodds, & R. Jaffe (2013). Dissolved black carbon in grassland
675 streams: Is there an effect of recent fire history? *Chemosphere, 90(10)*, 2557-2562.
676 http://10.1016/j.chemosphere.2012.10.098.
677 Ding, Y., K. M. Cawley, C. N. da Cunha, & R. Jaffe (2014). Environmental dynamics of
678 dissolved black carbon in wetlands. *Biogeochemistry, 119(1-3)*, 259-273.
679 https://doi.org/10.6084/m9.figshare.5571679.v4.
680 Ding, Y., Y. Yamashita, J. Jones, & R. Jaffe (2015). Dissolved black carbon in boreal forest and
681 glacial rivers of central Alaska: assessment of biomass burning versus anthropogenic
682 sources. *Biogeochemistry, 123(1-2)*, 15-25. https://doi.org/10.1007/s10533-014-0050-7.
683 Dittmar, T., C. E. de Rezende, M. Manecki, J. Niggemann, A. R. C. Ovalle, A. Stubbins, & M.
684 C. Bernardes (2012). Continuous flux of dissolved black carbon from a vanished tropical
685 forest biome. *Nature Geoscience, 5(9)*, 618-622. https://doi.org/10.1038/ngeo1541.
686 Fang, Y., B. Singh, B. P. Singh, & E. Krull (2014). Biochar carbon stability in four contrasting
687 soils. *European Journal of Soil Science, 65(1)*, 60-71. https://doi.org/10.1111/ejss.12094.
688 Fu, H. Y., H. T. Liu, J. D. Mao, W. Y. Chu, Q. L. Li, P. J. J. Alvarez, X. L. Qu, & D. Q. Zhu
689 (2016). Photochemistry of dissolved black carbon released from biochar: Reactive oxygen
690 species generation and phototransformation. *Environmental Science & Technology, 50(3)*,
691 1218-1226. https://doi.org/10.1021/acs.est.5b04314.
692 Glaser, B., & K. H. Knorr (2008). Isotopic evidence for condensed aromatics from non-
693 pyrogenic sources in soils - implications for current methods for quantifying soil black
694 carbon. *Rapid Communications in Mass Spectrometry, 22(7)*, 935-942.
695 https://doi.org/10.1002/rcm.3448.
696 Goranov, A., A. S. Wozniak, K. Bostick, A. R. Zimmerman, S. Mitra, & P. G. Hatcher
697 (Accepted). Photochemistry after fire: Structural transformations of pyrogenic dissolved

698 organic matter elucidated by advanced analytical techniques. *Geochimica et*
699 *Cosmochimica Acta.*
700 Guggenberger, G., W. Zech, & H. Schulten (1994). Formation and mobilization pathways of
701 dissolved organic matter: evidence from structural studies of organic matter fractions in
702 acid forest floor solutions. *Organic Geochemistry, 21*, 51-66. https://doi.org/10.1016/0146-
703 6380(94)90087-6.
704 Helms, J. R., A. Stubbins, J. D. Ritchie, E. C. Minor, D. J. Kieber, & K. Mopper (2008).
705 Absorption spectral slopes and slope ratios as indicators of molecular weight, source,and
706 photobleaching of chromophoric dissolved organic matter. *Limnology and Oceanography,*
707 *53(3)*, 955-969. https://doi.org/10.4319/lo.2008.53.3.0955.
708 Herlihy, L. J., J. N. Galloway, & A. Mills (1987). Bacterial utilization of formic and acetic acid
709 in rainwater. *Atmospheric Environment, 21(11)*, 2397-2402. https://doi.org/10.1016/0004-
710 6981(87)90374-X.
711 Higuchi, T. (2004). Microbial degradation of lignin: Role of lignin peroxidase, manganese
712 peroxidase, and laccase. *Proceedings of the Japan Academy Series B-Physical and*
713 *Biological Sciences, 80(5)*, 204-214. https://doi.org/10.2183/pjab.80.204.
714 Jaffé, R., Y. Ding, J. Niggemann, A. V. Vahatalo, A. Stubbins, R. G. M. Spencer, J. Campbell, &
715 T. Dittmar (2013). Global charcoal mobilization from soils via dissolution and riverine
716 transport to the oceans. *Science, 340(6130)*, 345-347. http://DOI:10.1126/science.1231476.
717 Jandl, R., & P. Sollins (1997). Water-extractable soil carbon in relation to the belowground
718 carbon cycle. *Biology and Fertility of Soils, 25*, 196-201.
719 https://doi.org/10.1007/s003740050303.
720 Johns, G. (2016). Austin Cary Forest Prescribed Burn, 33/8S/21E. *Prescribed Burn Prescription,*
721 *School of Forest Resources and Conservation, UF/IFAS*, 1-5.
722 Kaal, J., S. Wagner, & R. Jaffe (2016). Molecular properties of ultrafiltered dissolved organic
723 matter and dissolved black carbon in headwater streams as determined by pyrolysis-GC-
724 MS. *Journal of Analytical and Applied Pyrolysis, 118*, 181-191.
725 https://doi.org/10.1016/j.jaap.2016.02.003.
726 Kalbitz, K., J. Schmerwitz, D. Schwesig, & E. Matzner (2003a). Biodegradation of soil-derived
727 dissolved organic matter as related to its properties. *Geoderma, 113(3)*, 273-291.
728 https://doi.org/10.1016/S0016-7061(02)00365-8.

729 Kalbitz, K., D. Schwesig, J. Schmerwitz, K. Kaiser, L. Haumaier, B. Glaser, R. Ellerbrock, & P.
730 Leinweber (2003b). Changes in properties of soil-derived dissolved organic matter induced
731 by biodegradation. *Soil Biology and Biochemistry, 35(8)*, 1129-1142.
732 https://doi.org/10.1016/S0038-0717(03)00165-2.
733 Kappenberg, A., M. Blaesing, E. Lehndorff, & W. Amelung (2016). Black carbon assessment
734 using benzene polycarboxylic acids: Limitations for organic-rich matrices. *Organic*
735 *Geochemistry, 94*, 47-51. https://doi.org/10.1016/j.orggeochem.2016.01.009.
736 Keil, R. G., & D. L. Kirchman (1994). Abiotic transformation of labile protein to refractory
737 protein in seawater. *Marine Chemistry, 45*, 187-196. https://doi.org/10.1016/0304-
738 4203(94)90002-7.
739 Khodadad, C. L. M., A. R. Zimmerman, S. J. Green, S. Uthandi, & J. S. Foster (2011). Taxa-
740 specific changes in soil microbial community composition induced by pyrogenic carbon
741 amendments. *Soil Biology & Biochemistry, 43*, 385-392.
742 https://doi.org/10.1016/j.soilbio.2010.11.005.
743 Kieber, D. J., J. McDaniel, & K. Mopper (1989). Photochemical source of biological substrates
744 in sea water: Implications for carbon cycling. *Nature, 341*, 637-639.
745 https://doi.org/10.1038/341637a0.
746 Kiikkila, O., A. Smolander, & V. Kitunen (2013). Degradability, molecular weight and
747 adsorption properties of dissolved organic carbon and nitrogen leached from different types
748 of decomposing litter. *Plant and Soil, 373(1-2)*, 787-798. https://doi.org/10.1007/s11104-
749 013-1837-3.
750 Kim, S., D. A. Kaplan, & P. G. Hatcher (2006). Biodegradable dissolved organic matter in a
751 temperate and a tropical stream determined from ultra–high resolution mass spectrometry.
752 *Limnology and Oceanography, 51(2)*, 1054-1063.
753 https://doi.org/10.4319/lo.2006.51.2.1054.
754 Kolb, S., & A. Stacheter (2013). Prerequisites for amplicon pyrosequencing of microbial
755 methanol utilizers in the environment. *Frontiers in Microbiology, 4*, 268.
756 https://doi.org/10.3389/fmicb.2013.00268.
757 Lee, Y., B. Lee, J. Hur, J.-O. Min, S.-Y. Ha, K. Ra, K.-T. Kim, & K.-H. Shin (2016).
758 Biodegradability of algal-derived organic matter in a large artificial lake by using stable

isotope tracers. *Environmental Science and Pollution Research, 23(9)*, 8358-8366. https://doi.org/10.1007/s11356-016-6046-1.

Lin, Y., S. D. Karlen, J. Ralph, & J. Y. King (2018). Short-term facilitation of microbial litter decomposition by ultraviolet radiation. *Science of The Total Environment, 615*, 838-848. http://10.1016/j.scitotenv.2017.09.239.

Lindell, M. J., W. Granee`li, & L. J. Tranvik (1995). Enhanced bacterial growth in response to photochemical transformation of dissolved organic matter. *Limnology and Oceanography, 40*, 195-199. https://doi.org/10.4319/lo.1995.40.1.0195.

Mann, P. J., et al. (2013). Evidence for key enzymatic controls on metabolism of Arctic river organic matter. *Global Change Biology, 20(4)*, 1089-1100. https://doi.org/10.1111/gcb.12416.

Marschner, B., & K. Kalbitz (2003). Controls of bioavailability and biodegradability of dissolved organic matter in soils. *Geoderma, 113(3)*, 211-235. https://doi.org/10.1016/S0016-7061(02)00362-2.

McGinnis, G. D., H. Boraazjani, L. K. McFarland, & D. A. Strobel (1988). Characterisation and laboratory testing soil treatability studies for creosote and pentachlorophenol sludges and contaminated soil. *USEPA, Report No. 60/2-88/055*. https://nepis.epa.gov/Exe/ZyPURL.cgi?Dockey=20012OKA.TXT.

Miller, W. L., & M. A. Moran (1997). Interaction of photochemical and microbial processes in the degradation of refractory dissolved organic matter from a coastal marine environment. *Limnology and Oceanography, 42(6)*, 1317-1324. https://doi.org/10.4319/lo.1997.42.6.1317.

Moran, M. A., & R. G. Zepp (1997). Role of photoreactions in the formation of biologically labile compounds from dissolved organic matter. *Limnology and Oceanography, 42(6)*, 1307-1316. https://doi.org/10.4319/lo.1997.42.6.1307.

Mukherjee, A., & A. R. Zimmerman (2013). Organic carbon and nutrient release from a range of laboratory-produced biochars and biochar-soil mixtures. *Geoderma, 193*, 122-130. https://doi.org/10.1016/j.geoderma.2012.10.002.

Myers-Pigg, A. N., P. Louchouarn, W. Amon, A. Prokushkin, K. Piece, & A. Rubtsov (2015). Labile pyrogenic dissolved organic carbon in major Siberian Arctic rivers: Implications for

wildfire-stream metabolic linkages. *Geophysical Research Letters, 42*, 377-385. https://doi.org/10.1002/2014GL062762.

Nierop, K. G. J., C. M. Preston, & J. M. Verstraten (2006). Linking the B ring hydroxylation pattern of condensed tannins to C, N and P mineralization. A case study using four tannins. *Soil Biology & Biochemistry, 38(9)*, 2794-2802. https://doi.org/10.1016/j.soilbio.2006.04.049.

Norwood, M. J., P. Louchouarn, L. J. Kuo, & O. R. Harvey (2013). Characterization and biodegradation of water-soluble biomarkers and organic carbon extracted from low temperature chars. *Organic Geochemistry, 56*, 111-119. 10.1016/j.orggeochem.2012.12.008.

Payne, C. M., B. C. Knott, H. Mayes, H. Hansson, M. E. Himmel, M. Sandgren, J. Stahlberg, & G. Beckham (2015). Fungal cellulases. *Chemical Reviews, 115(3)*, 1208-1448. https://doi.org/10.1021/cr500351c.

Qualls, R. G. (2005). Biodegradability of dissolved organic from decomposing fractions of carbon leached leaf litter. *Environmental Science & Technology, 39(6)*, 1616-1622. http://10.1021/es049090o.

Qualls, R. G., & B. L. Haines (1992). Biodegradability of dissolved organic in forest throughfall, soil solutions, and stream water. *Soil Science Society of America Journal, 56(2)*, 578-586. http://10.2136/sssaj1992.03615995005600020038x.

Roebuck, J. A., D. C. Podgorksi, S. Wagner, & R. Jaffe (2017). Photodissolution of charcoal and fire-impacted soil as a potential source of dissolved black carbon in aquatic environments. *Organic Geochemistry, 112*, 16-21. http://10.1016/j.orggeochem.2017.06.018.

Rossel, P. E., A. V. Va¨ha¨talo, M. Witt, & T. Dittmar (2013). Molecular composition of dissolved organic matter from a wetland plant (Juncus effusus) after photochemical and microbial decomposition (125 year): common features with deep sea dissolved organic matter. *Organic Geochemistry, 60*, 62-71. http://10.1016/j.orggeochem.2013.04.013.

Schwesig, D., K. Kalbitz, & E. Matzner (2003). Mineralization of dissolved organic carbon in mineral soil solution of two forest soils. *Journal of Plant Nutrition and Soil Science, 166(5)*, 585-593. http://10.1002/jpln.200321103.

818 Sims, R. C., W. J. Doucette, J. E. McLean, W. J. Grenney, & R. R. Dupont (1988). Treatment
819 potential for 56 EPA listed hazardous chemicals in soil. *USEPA, Report No. 600/6-88/001*.
820 https://cfpub.epa.gov/si/si_public_record_Report.cfm?Lab=ORD&dirEntryID=46060.
821 Sorrenti, G., C. A. Masiello, B. Dugan, & M. Toselli (2016). Biochar physico-chemical
822 properties as affected by environmental exposure. *Science of The Total Environment, 563*,
823 237-246. http://10.1016/j.scitotenv.2016.03.245.
824 Spencer, R. G. M., P. J. Mann, T. Dittmar, T. I. Eglinton, C. McIntyre, R. Max Holmes, N.
825 Zimov, & A. Stubbins (2015). Detecting the signature of permafrost thaw in Arctic rivers.
826 *Geophysical Research Letters, 42*, 2830-2835. http://doi:10.1002/2015GL063498.
827 Spencer, R. G. M., et al. (2009). Photochemical degradation of dissolved organic matter and
828 dissolved lignin phenols from the Congo River. *Journal of Geophysical Research-*
829 *Biogeosciences, 114*, 1-12. 10.1029/2009jg000968.
830 Strauss, E. A., & G. A. Lamberti (2002). Effect of dissolved organic carbon quality on microbial
831 decomposition and nitrification rates in stream sediments. *Freshwater Biology, 47(1)*, 65-
832 74. http://10.1046/j.1365-2427.2002.00776.x.
833 Stubbins, A., J. Niggemann, & T. Dittmar (2012a). Photo-lability of deep ocean dissolved black
834 carbon. *Biogeosciences, 9(5)*, 1661-1670. http://10.5194/bg-9-1661-2012.
835 Stubbins, A., et al. (2012b). Anthropogenic aerosols as a source of ancient dissolved organic
836 matter in glaciers. *Nature Geoscience, 5(3)*, 198-201. 10.1038/ngeo1403.
837 Tejirian, A., & F. Xu (2011). Inhibition of enzymatic cellulolysis by phenolic compounds.
838 *Enzyme and Microbial Technology, 48*, 239-247.
839 https://doi.org/10.1016/j.enzmictec.2010.11.004.
840 Tian, J. H., P. A. M., & T. Bouchez (2014). Occurrence of lignin degradation genotypes and
841 phenotypes among prokaryotes. *Applied Microbiology and Biotechnology, 98*, 9527-9544.
842 https://doi.org/10.1007/s00253-014-6142-4.
843 Tranvik, L., & S. Kokalj (1998). Decreased biodegradabihty of algal DOC due to interactive
844 effects of UV radiation and humic matter. *Aquatic Microbial Ecology, 14*, 301-307.
845 http://doi:10.3354/ame014301.
846 van Hees, P. A. W., D. L. Jones, R. Finlay, D. L. Godbold, & U. S. Lundström (2005). The
847 carbon we do not see—the impact of low molecular weight compounds on carbon

dynamics and respiration in forest soils: a review. *Soil Biology and Biochemistry, 37(1)*, 1-13. http://doi.org/10.1016/j.soilbio.2004.06.010.

Vujinović, T., T. J. Clough, D. Curtin, E. D. Meenken, N. J. Lehto, & M. H. Beare (2019). Quantity and biodegradability of dissolved organic matter released from sequentially leached soils, as influenced by the extent of soil drying prior to rewetting. *Soil Research, 57(4)*, 374-386. http://doi.org/10.1071/SR18172.

Waggoner, D. C., H. M. Chen, A. S. Willoughby, & P. G. Hatcher (2015). Formation of black carbon-like and alicyclic aliphatic compounds by hydroxyl radical initiated degradation of lignin. *Organic Geochemistry, 82*, 69-76. http://10.1016/j.orggeochem.2015.02.007.

Wagner, S., R. Jaffe, & A. Stubbins (2018). Dissolved black carbon in aquatic ecosystems. *Limnology and Oceanography, 3*, 168-185. 10.1002/lol2.10076.

Ward, C. P., R. L. Sleighter, P. G. Hatcher, & R. M. Cory (2014). Insights into the complete and partial photooxidation of black carbon in surface waters. *Environ Sci Process Impacts, 16(4)*, 721-731. 10.1039/c3em00597f.

Ward, C. P., S. G. Nalven, B. C. Crump, G. Kling, & R. Cory (2017). Photochemical alteration of organic carbon draining permafrost soils shifts microbial metabolic pathways and stimulates respiration. *Nature Communications, 8*, 1-8. http://10.1038/s41467-017-00759-2.

Wetzel, R. G., P. G. Hatcher, & T. S. Bianchi (1995). Natural photolysis by ultraviolet irradiance of recalcitrant dissolved organic matter to simple substrates for rapid bacterial metabolism. *Limnology and Oceanography, 40(8)*, 1369-1380. http://10.4319/lo.1995.40.8.1369.

Whitty, S. D., D. C. Waggoner, R. M. Cory, L. A. Kaplan, & P. G. Hatcher (2019). Direct noninvasive 1H NMR analysis of stream water DOM: Insights into the effects of lyophilization compared with whole water. *Magnetic Resonance in Chemistry*, 1-14. https://doi.org/10.1002/mrc.4935.

Wolter, M., F. Zadrazil, R. Martens, & M. Bahadir (1997). Degradation of eight highly condensed polycyclic aromatic hydrocarbons by Pleurotus sp. Florida in solid wheat straw substrate. *Applied Microbiology and Biotechnology, 48*, 398-404. https://doi.org/10.1007/s002530051070.

Wozniak, A. S., R. L. Sleighter, H. Abdulla, A. S. Priest, P. L. Morton, R. U. Shelley, W. M. Landing, & P. G. Hatcher (2013). Relationships among aerosol water soluble organic

matter, iron and aluminum in European, North African, and Marine air masses from the 2010 US GEOTRACES cruise. *Marine Chemistry*, *154*, 24-33. https://doi.org/10.1016/j.marchem.2013.04.011.

Wozniak, A. S., A. I. Goranov, S. Mitra, K. W. Bostick, A. R. Zimmerman, D. R. Schlesinger, S. Myneni, & P. G. Hatcher (2020). Molecular Heterogeneity in Pyrogenic Dissolved Organic Matter From A Thermal Series of Oak and Grass Chars. *Organic Geochemistry*, 104065. https://doi.org/10.1016/j.orggeochem.2020.104065.

Zimmerman, A. (2010). Abiotic and microbial oxidation of laboratory-produced black carbon (biochar). *Environmental Science and Technology, 44*, 1295-1301. https://doi.org/10.1021/es903140c.

Zimmerman, A. R., & L. Ouyang (2019). Priming of pyrogenic C (biochar) mineralization by dissolved organic matter and vice versa. *Soil Biology & Biochemistry, 130*, 105-112. https://doi.org/10.1016/j.soilbio.2018.12.011.

Zimmerman, A. R., B. Gao, & M.-Y. Ahn (2011). Positive and negative carbon mineralization priming effects among a variety of biochar-amended soils. *Soil Biology & Biochemistry, 43*, 1169– 1179.

Ziolkowski, L. A., & E. R. M. Druffel (2010). Aged black carbon identified in marine dissolved organic carbon. *Geophysical Research Letters, 37*, 1-4. http://10.1029/2010gl043963.

Ziolkowski, L. A., A. R. Chamberlin, J. Greaves, & E. R. M. Druffel (2011). Quantification of black carbon in marine systems using the benzene polycarboxylic acid method: a mechanistic and yield study. *Limnology and Oceanography-Methods, 9*, 140-149. http://10.4319/lom.2011.9.140.

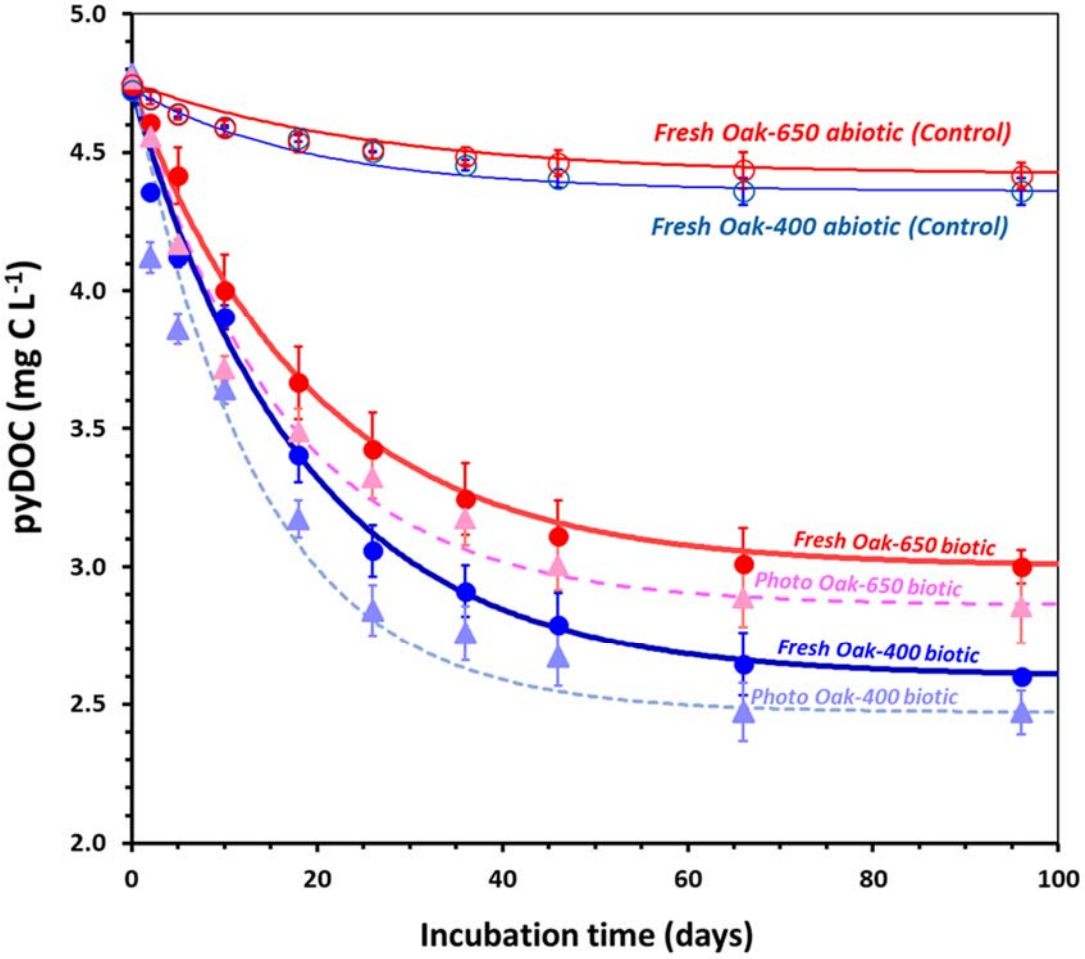

Figure 1. Pyrogenic dissolved organic carbon (pyDOC) concentrations in fresh and photodegraded Oak-400 and Oak-650 char leachates during the microbial and abiotic incubations. Curves represent the modelled exponential decay (model parameters given in Table 1).

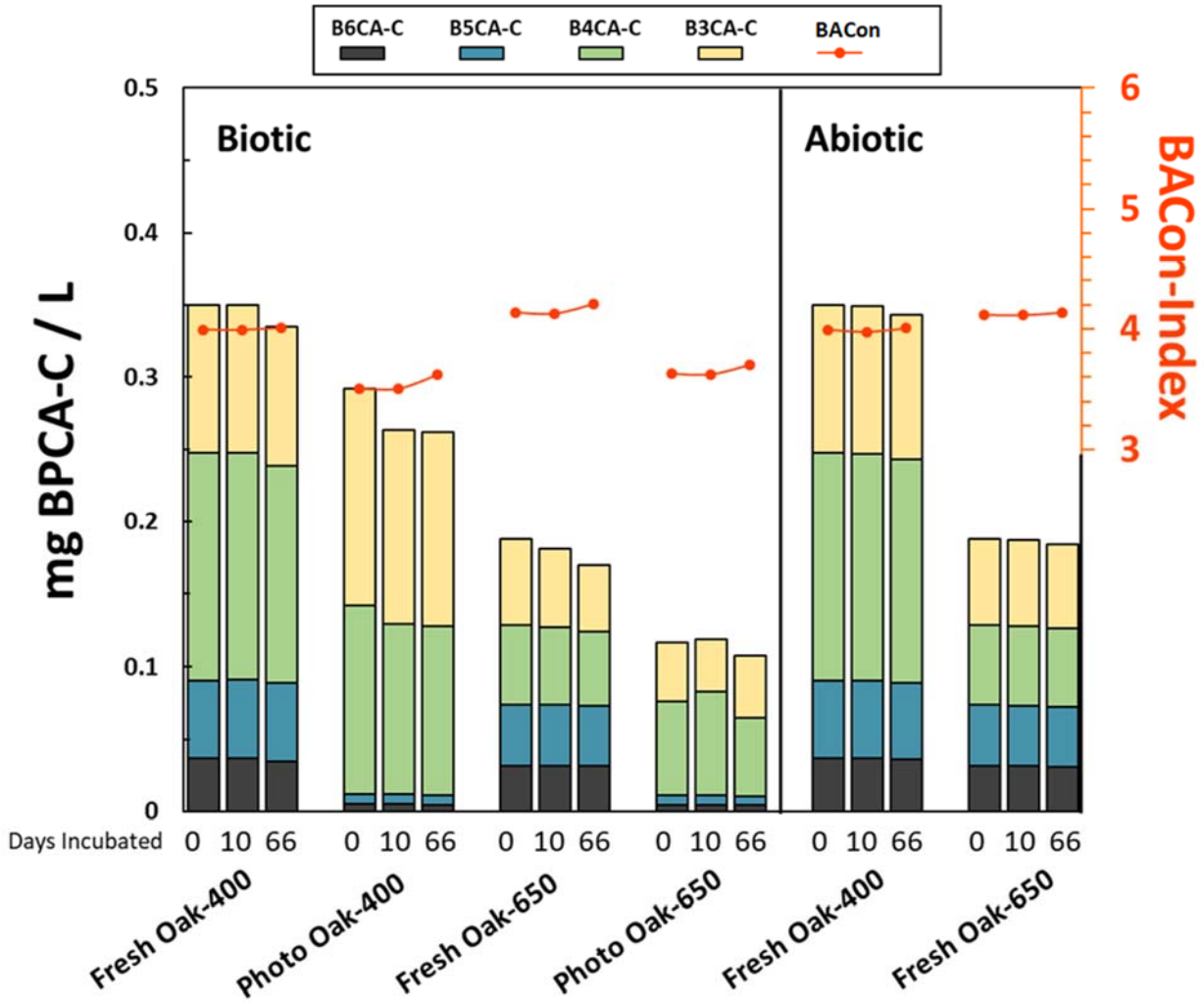

907

908 **Figure 2**. Distribution of BPCA-C compounds produced by initial and incubated (days 10 and
909 66) oak char leachates (left y-axis, bar graphs) and BPCA Aromatic Condensation (BACon)
910 Index, i.e. average number of carboxyl groups among the BPCA compounds, representing degree
911 of aromatic condensation (right y-axis, orange datapoints).

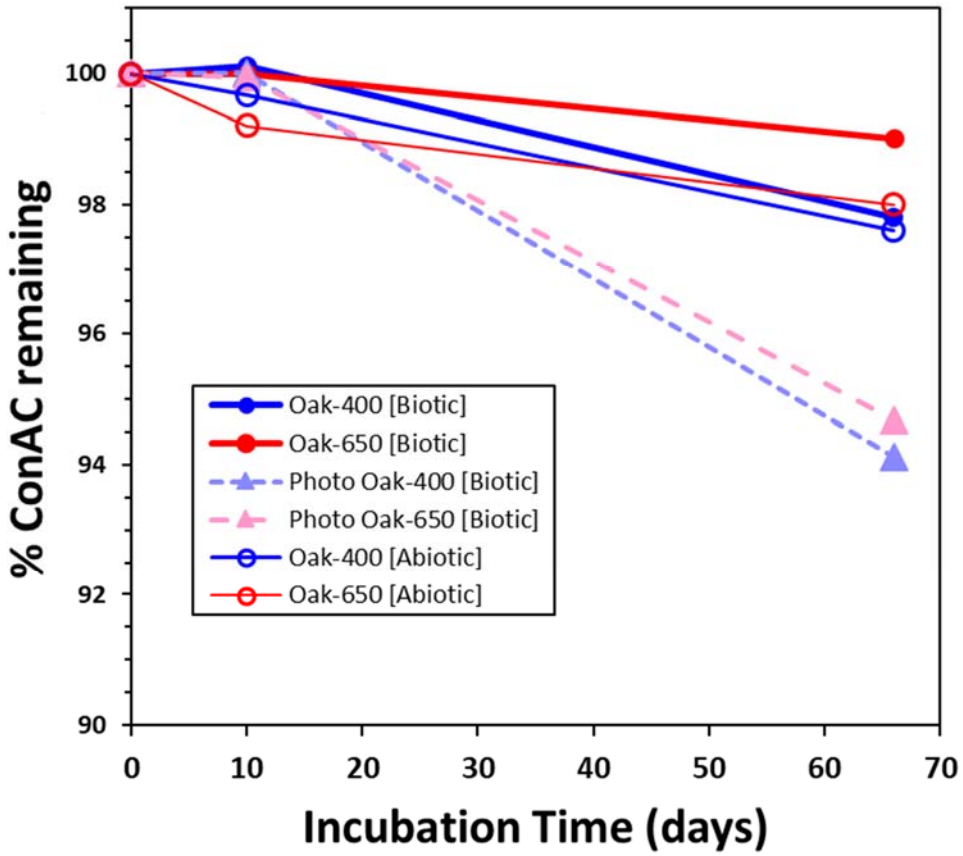

912

913 **Figure 3**. Relative condensed aromatic carbon (ConAC) content (% of initial ConAC content) of

914 fresh and photodegraded oak char leachates during microbial and abiotic incubations.

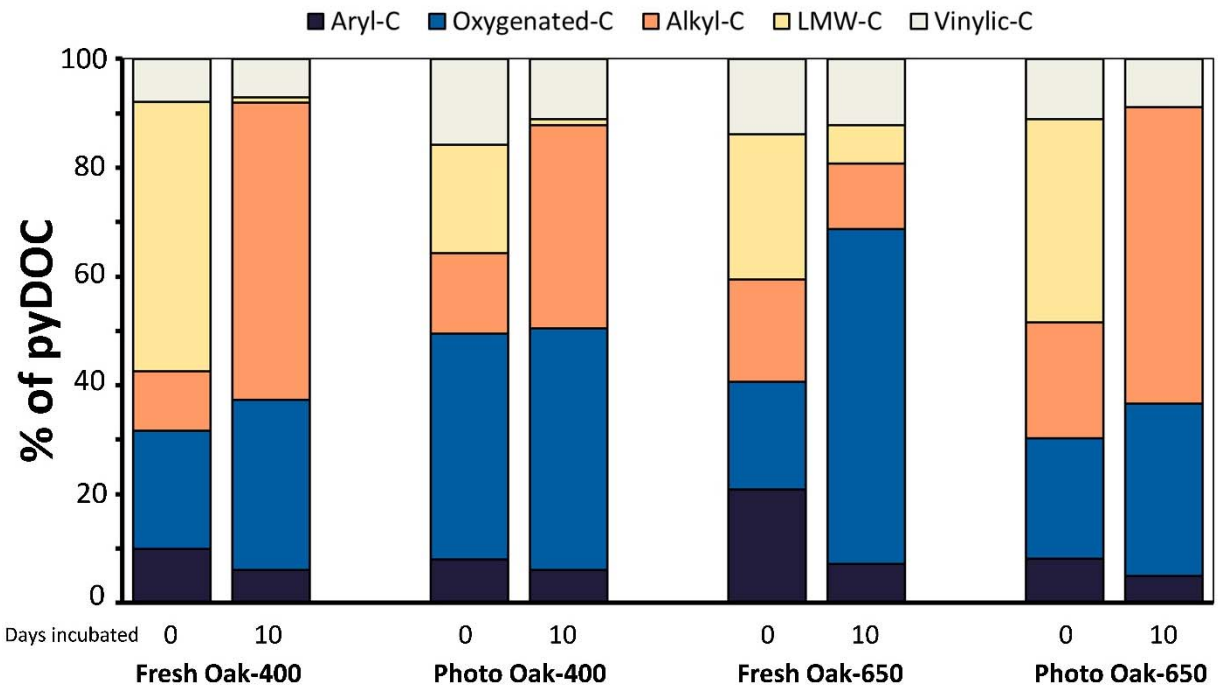

915

916 **Figure 4**. Relative abundance of carbon in different functional groups, calculated using ^{1}H-NMR
917 data, in initial and 10-day microbially-incubated Oak-400 and Oak-650 char leachates. See the
918 text for details on chemical group assignment and conversion to C units.

919

920

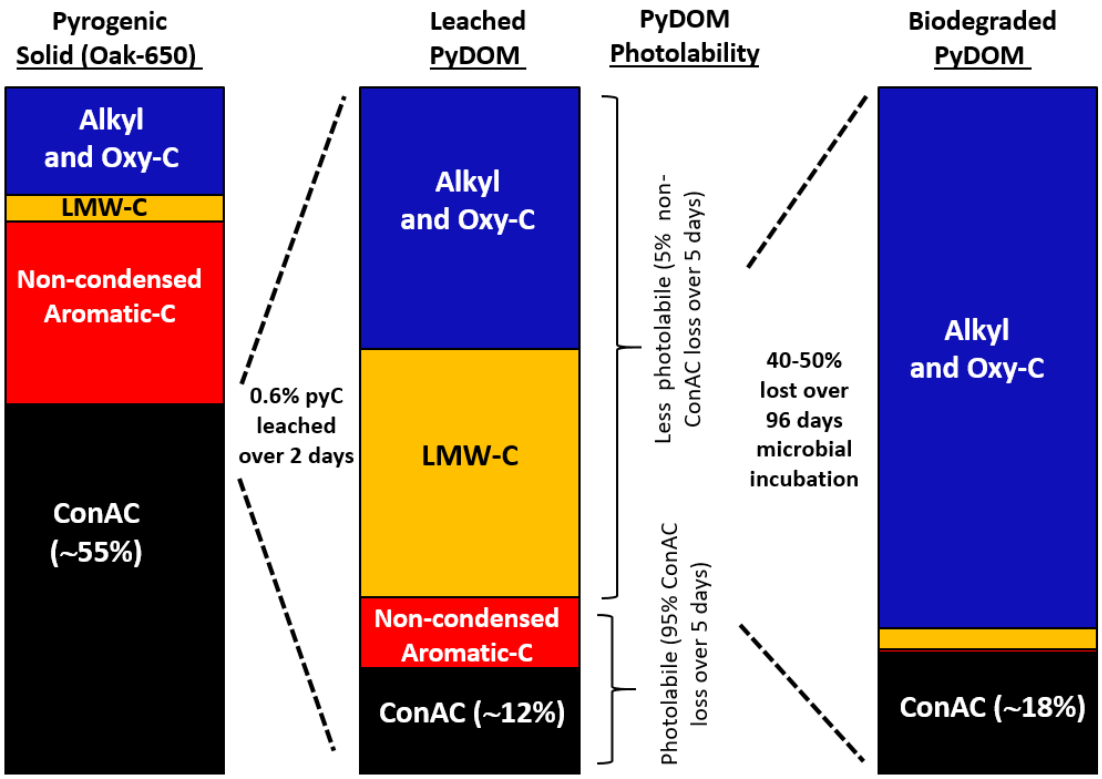

921
922

923 **Figure 5**. Summary diagram showing generalized trends in production (from Bostick et al.,
924 2018) and transformation of pyDOM via photo- (from Bostick at al., 2020) and biodegradation
925 (this study). Relative abundance of functional group carbon is calculated using 1H-NMR data,
926 reported on a carbon basis as well as ConAC which is estimated using B5CA and B6CA
927 molecular markers.

928

929 **Table 1**. First-order exponential decay model parameters for mineralizable pyDOC portion (all

930 with r^2>0.98 fits).

Leachate	*Modeled Mineralizable pyDOC fraction (%)*	*k* (y^{-1})	$t_{1/2}$ (d)
Fresh Oak-400 Biotic	45	19.72	12.4
Photo Oak-400 Biotic	48	27.05	9.3
Fresh Oak-650 Biotic	37	18.94	13.4
Photo Oak-650 Biotic	41	22.74	11.0
Fresh Oak-400 Abiotic	7	13.84	18.3
Fresh Oak-650 Abiotic	8	19.10	13.2

931

932 Notes

933 *k* = first order loss rate constant of the biodegradable portion

934 $t_{1/2}$ = the half-life of the mineralizable pyDOC in the experimental system

935

936